TROPOMI/S5P sensitivity limits with respect to detection of NO_2 plumes from seagoing ships

Solomiia Kurchaba
s.kurchaba@liacs.leidenuniv.nl,@k_solomiia
Twitter:@k_solomiia
Leiden University
Leiden Institute of Advanced
Computer Science (LIACS)
Leiden, The Netherlands

Artur Sokolovsky
Newcastle University
School of Computing
Newcastle-upon-Tyne, UK

Jasper van Vliet
Human Environment and Transport
Inspectorate (ILT)
Utrecht, The Netherlands

Fons J. Verbeek
Leiden University
Leiden Institute of Advanced
Computer Science (LIACS)
Leiden, The Netherlands

Cor J. Veenman
Leiden University
Leiden, The Netherlands
Data Science Department, TNO
The Hague, The Netherlands

ABSTRACT

The marine shipping industry is among the strong emitters of nitrogen oxides (NO_x) – a substance harmful to ecology and human health. Monitoring of emissions from shipping is a significant societal task. Currently, the only technical possibility to observe NO_2 emission from seagoing ships is using TROPOMI/S5P satellite data. A range of studies reported that NO_2 plumes from some individual ships can be visually distinguished on selected TROPOMI images. However, all these studies applied subjectively established pre-determined thresholds to the minimal speed/length of the ship – variables that to a large extent define the emission potential of a ship. In this study, we investigate the sensitivity of the TROPOMI sensor with respect to the NO_2 emitted by individual seagoing ships of a certain speed/length. For this, we train a classification model to distinguish TROPOMI patches with a ship, from the patches, where there were no ships. In order to test for regional differences, we study four regions: the Mediterranean Sea, Biscay Bay, Arabian Sea, and Bengal Bay. For the Mediterranean and the Arabian Sea, we estimate the TROPOMI sensitivity limit to lie around a minimal speed of 10 kt and a minimal length of 150 m. We further show that when focusing the analysis on bigger emitters, the detectability of NO_2 plumes can be improved up to 0.8 ROC-AUC. However, the rate of improvement is dependent on the region studied. Finally, we show that increasing the size of the dataset, beyond the dataset used in this study, will likely yield further improvements in the detectability of smaller/slower ships. This paper is the first comprehensive study on the real-world sensitivity of the TROPOMI instrument to distinguish the NO_2 emission produced by seagoing ships.

KEYWORDS

TROPOMI, sensitivity limits, machine learning, emissions, seagoing ships, NO2

1 INTRODUCTION

International shipping is one of the biggest emitters of nitrogen oxides (NO_x). The increased abundance of these gases in the atmosphere causes severe damage to human health and ecology [5]. In order to mitigate the negative effects caused by the industry, International Maritime Organization (IMO) introduced incremental restrictions on emission levels that can be produced by individual seagoing ships [13, 14]. However, the methods currently used for ship emission monitoring such as on-board [1], in-situ [2, 20], and airborne platform-based measurements [24] require close proximity to a ship, and, therefore, do not allow performing monitoring in the open sea and on a global scale.

Several studies reported that with the TROPOspheric Monitoring Instrument on board the Copernicus Sentinel 5 Precursor (TROPOMI/S5P) satellite [25], some plumes from individual ships can be visually distinguished [8, 10, 15, 16]. However, in all studies, the authors applied a pre-determined threshold on the minimal speed/length of the ship – the variables that are determinants of the level of ship emission potential. For instance, in [10] the authors studied several days of TROPOMI measurements in the Mediterranean Sea, while visually analyzing ship plumes from ships longer than 200 meters. In [15], a threshold-based ship plume segmentation approach was applied on several days of measurement from the Arabian and Mediterranean seas. The studied ships were longer than 150 meters and sailed faster than 12 knots. In [16], a machine-learning-based ship plume segmentation model was applied to eight months of TROPOMI measurements. While the approach allows quantification of emission intensity, only ships with a speed above 14 knots were analyzed. In [8], the authors scanned the globe with the machine-learning-based classifier to identify visually distinguishable NO_2 plumes. Some of the detected plumes corresponded with the known shipping lanes. Nevertheless, the study did not provide any information on the parameters of the ships from which the NO_2 plumes were detected. To sum up, to this moment, there is no study that investigates the global/regional sensitivity of the TROPOMI sensor with respect to the NO_2 emission produced by individual seagoing ships related to their speed and length.

In this study, we investigate the sensitivity limits of the TROPOMI instrument with respect to the detection of NO_2 plumes from seagoing ships. To tackle this problem, we train a machine learning classification model to distinguish image patches covering the area with at least one ship from the image patches of the area where there were no ships. Given the trained classification model, we address the following research questions: **RQ1**: What is the minimal speed/length of the seagoing ship so that the NO_2 plume from it can be detected with the TROPOMI/S5P instrument? **RQ2**: To what extent can the detectability of NO_2 plumes be improved if only the biggest emitters are taken into account? **RQ3**: Is there a potential for improvement of detectability of NO_2 plumes from the slow/small ships if more data would be used to train the used classification model?

The study is conducted on four regions of interest: Mediterranean Sea, Biscay Bay, Arabian Sea, and Bengal Bay (the coordinate scope see in Table 1 and Figure 1). The study areas are directed towards the Europe – Middle East – Asia trade route, with selected areas representing low background pollution and common occurrence of clear skies. This is the first comprehensive study on the sensitivity of the TROPOMI instrument to the NO_2 emission produced by seagoing ships.

The rest of the paper is organized as follows: In Section 2, we introduce the used data sources and explain how the data was preprocessed in order to obtain datasets used for machine learning models. In Section 3, we explain the experimental setup for each stage of the study and present the obtained results. We then present the discussion of the obtained results in Section 4, and conclude in Section 5.

2 DATA

We create the dataset by combining the data from several sources: 1) the TROPOMI/S5P NO_2 measurements, 2) wind information, and 3) AIS (Automatic Identification System) data on ship positions. The dataset is prepared for supervised machine learning to identify ship plumes on image patches. In this Section, we describe all steps of the data preparation.

2.1 Data sources

Our main source of the data is the TROPOMI/S5P instrument. This is a UV-Vis-NIR-SWIR (UV, visible, near-infrared, short-wave infrared) spectrometer with the maximal ground pixel resolution of 3.5×5.5 km^2 at nadir. The TROPOMI instrument is on board the Sentinel-5 satellite mission – a sun-synchronous satellite with a local equatorial overpass time at 13:30. The TROPOMI instrument measures an extensive list of trace gases. In this study, we focus our attention on the NO_2 product (TROPOMI data version: 2.4.0.). Previous studies [8, 10, 15–17] showed that with this data product, we can distinguish emission plumes from some individual seagoing ships. The NO_2 gas is a result of photochemical reactions of NO_x emitted by ships, which allows it to be used for ship emission monitoring. The trace gas variable of our interest is *Tropospheric Slant Column Density – SCD trop* [6]. In contrast to vertical column density (VCD), which was used for instance in [15, 16], the derivation of SCD is not based on airmass factor – a variable estimated using, among others, information about historical NO_2 concentration within a certain area. Since *SCD trop* does not contain information about historical NO_2 concentrations, it is suitable for the study of satellite sensitivity [10].

Information about wind speed and direction, which is crucial for understanding plume dispersion, is taken from wind speed data from the European Center for Medium-range Weather Forecast (ECMWF) at 10 m height, available with 0.25° resolution at a 6-hourly time step. The data is available as a support product in a TROPOMI file.

The data on ship positions is obtained through Automatic Identification System (AIS) transponders[1]. Among others, the data include the position, speed, and unique identifier (MMSI) of each ship carrying an active transponder. Information about the dimensions of the ships is obtained from the official ship registries[2].

2.2 Data preprocessing

The first step of data preparation is regridding[3]. This is done so that for each region we have pixels with the same spatial coverage. The regridded pixel size for each region is approximately equal to 4×5 km^2. Following the set-up used in the previous studies [16, 17], for the regridding, we only use pixels with cloud coverage below 0.5, wind speed lower than 10 [m/s], and *qa value* [22] above 0.5. Such filtering criteria is a trade-off between a high standard of data quality, and attempts of preservation of as many data points as possible.

As a next step, we split the studied area into non-overlapping patches of equal size 80×80 km^2. The selected size of the image corresponds to a distance that the fastest ships in the dataset will cover in 2 hours. The observation period of 2 hours was motivated by the fact that due to the physical dispersion and limited lifetime of NO2 within plumes, the detectability of ship plumes will fall sharply after 2 hours [26]. For each image patch, we calculate how many ships were in the central area of the patch within 2 hours before the overpass of the satellite. The central area of the patch is defined as 60×60 km^2 square. An example of a set-up used for counting the number of ships within an image patch is presented in Figure 2. The resulting distribution of the number of ships per image patch for each studied region can be found in Figure 3. Please note the regional differences in the distribution of ships among patches. The Arab Sea typically has a high number of patches with a single ship. The Biscay Bay, in comparison to other regions, has the highest number of patches with a high number of ships on it. These patterns illustrate the difference in shipping density among the studied regions.

2.3 Dataset preparation

To study the sensitivity of the TROPOMI satellite with respect to the detection of NO_2 plumes from seagoing ships, we prepare a dataset for supervised machine learning. The objective is to distinguish image patches that cover the area where there was no ship, from image patches covering the area with at least one ship on it. Since

[1] As of 2002 all commercial sea-going vessels are required to carry on board an AIS transponder [21].

[2] Since at the moment there is no open-access AIS data available, for the scope of this study, the AIS data, as well as information about the dimensions of the ships, were provided by the Netherlands Human Environment and Transport Inspectorate (ILT)

[3] The regridding is performed using the Python package HARP v.1.13.

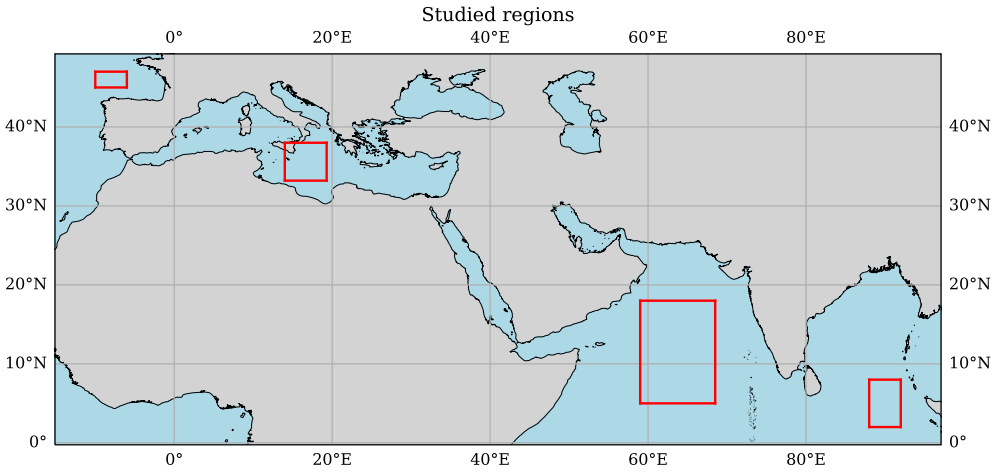

Figure 1: Red squares indicate bounding boxes of the four studied regions (from left to right): Biscay Bay, Mediterranean Sea, Arabian Sea, Bengal Bay.

Region	Longitude [deg]	Latitude [deg]	Studied period
Mediterranean	(14, 19.3)	(33.2, 38)	(31-03-20; 28-02-23)
Biscay Bay	(-10, -6)	(45, 47)	(01-04-20; 28-02-23)
Arabian Sea	(59, 68.5)	(5, 18)	(31-03-20; 30-11-22)
Bengal Bay	(88, 92)	(2, 8)	(03-06-20; 31-12-22)

Table 1: Geographical coordinates and analyzed periods defining the study scope for each region.

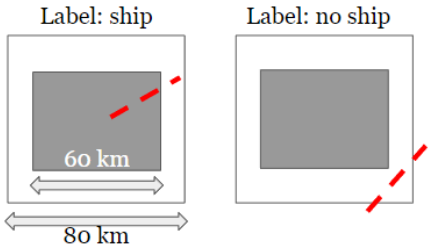

Figure 2: An illustration of the set-up used for counting the number of ships per image patch. White square – image patch. Black square – a central part of the image patch. Red dashed lines – ship trajectory starting from 2 hours before until the moment of the satellite overpass. Only ships, whose trajectories cross the central part of the image patch are considered to be present in the area covered by a patch.

this is a binary problem, the value of the target will be 1, if there is at least one ship, which is faster than 6 kt (11.1 km/h) and longer than 90 meters in the area covered by an image patch. The target value is 0, if there is no ship in the area, or the ship is shorter than 90 meters or slower than 6 kt. The values of 90 meters and 6 kt are sufficiently low to be well below detectable limits as this study will show. The resulting distribution of classes for studied regions can be found in Table 2. Examples of image patches without (label 0) and with at least one ship on it (label 1) can be found in Appendix A.

Region	Ship image	No ship image
Mediterranean	6652	9693
Biscay Bay	2641	2812
Arabian Sea	4804	24594
Bengal Bay	2444	6848

Table 2: Class-wise distribution of image patches for each studied region. The rate of imbalance depends on the traffic density in the region.

We address the classification problem with a multivariate classifier. Therefore, we represent the TROPOMI image patches in terms of a set of features - a statistical representation of the image patch. More specifically, for the regridded pixels of each image patch, we calculate the following statistics: *min(SCD), mean(SCD), median(SCD), max(SCD), std(SCD)*, where SCD stands for NO_2 slant column density. To give information about the level of plume dispersion, we add wind-related variables *zonal wind velocity (wind zon), meridional wind velocity (wind med)*, which represent the speed of the wind from the west to east and from south to north respectively. Finally, we add features *sensor zenith angle* and *solar azimuth angle* to represent the viewing geometry of the satellite. Values for wind information and satellite geometry are the average values

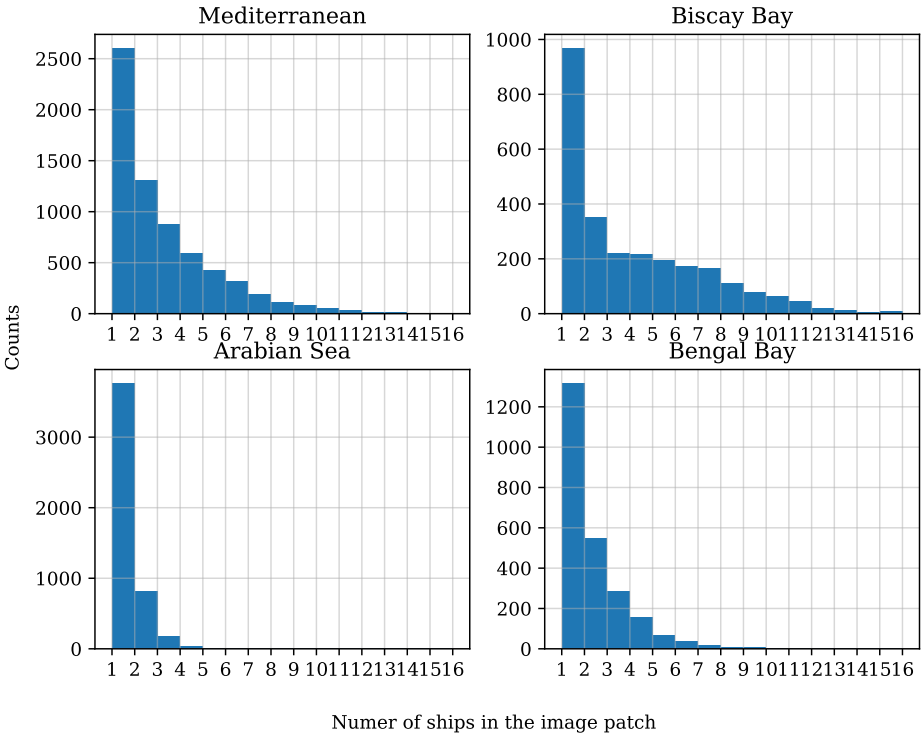

Figure 3: Distribution of ship number per image patch for the studied regions.

Feature type	Feature name
NO_2 slant column density	min(SCD)
	mean(SCD)
	median(SCD)
	max(SCD)
	std(SCD)
Wind information	zonal wind velocity
	meridional wind velocity
Satellite geometry	sensor zenith angle
	solar azimuth angle

Table 3: List of features used for classification model.

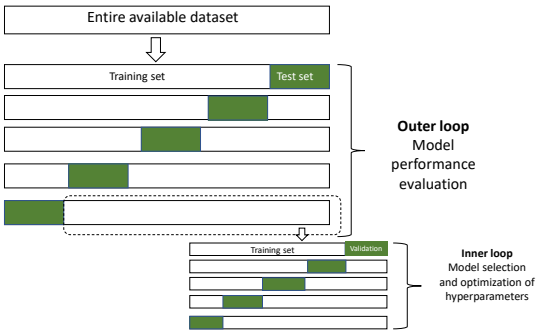

Figure 4: Nested cross-validation. Applied scheme of hyperparameter optimization and model selection. Source: [17].

of the pixels within the image patch. The resulting feature set is presented in Table 3. In Appendix B, the reader can find histograms of the dataset features for the studied regions. We would also like to remind the reader that features related to the properties of ships cannot be included in the feature space. Moreover, we deliberately do not include any features in the feature set related to the geographic locations of a given patch. This is because within a studied area there might be preferred routes that are taken by ships more often. In this situation, information about the geographic locations may bias the model. Prior to being used by the machine learning model, all features were normalized using a RobustScaler [7] from scikit-learn v.1.2.2.

3 EXPERIMENTS AND RESULTS

In this Section, we describe the experiments and show the results obtained. We start with the introduction of the classification model – we present model selection and hyperparameter optimization results. For the selected model, we provide the explainability analysis. Next, in the consecutive subsections, we explain and provide the results of the experiments addressing the three research questions of this study.

3.1 Classification model

3.1.1 Experimental setup. As a first step, we compare the performance of several multivariate classifiers, in order to select the one that is going to be used in the remaining part of the paper for the TROPOMI sensitivity analysis. We study four machine learning classifiers of increasing complexity: Logistic regression, Support Vector Machine (SVM) with the radial basis function (rbf) kernel, Random Forest[4], and Extreme Gradient Boosting[5] (XGB) [4]. All selected models are robust to noise and can be efficient even given the relatively small size of datasets. To make sure that we exploit the maximal potential of a given machine learning model, we optimize the hyperparameters of each studied model. The hyperparameters are optimized using a random search[6] technique with the objective metrics - *average precision*. The used search space of the hyperparameters for each of the studied models is provided in Appendix C. To be able to simultaneously perform the hyperparameter optimization and evaluation of the model performance, we use 5-fold nested cross-validation [3, 23] (see Figure 4 for visual explanation). To maintain the same percentage of samples of a certain label in the training and test set, the cross-validation was based on *stratified Kfold* split [11, 12]. The set of hyperparameters yielding the best results at each iteration of cross-validation is provided in Appendix D.

3.1.2 Results. The classification results are presented in Table 4. The model that yielded the best results for most of the regions is XGB. Therefore, this model will be used for the rest of the experiments of this study. Further analyzing the results, we can observe the correspondence of the level of achieved ROC-AUC (Area Under Reciever Operating Characteristics Curve) scores per region with the number of ships per image patch presented in Figure 3. Due to the different rates of class imbalance though, the average precision scores cannot be compared across the regions. Further, in Figure 5, for each studied region, we present the precision-recall and ROC curves obtained using the optimized XGB model. Here, we also observe that the model performance for the regions Mediterranean Sea, and Biscay Bay is better than for the Arabian Sea, and Bengal Bay.

3.1.3 Explainability analysis. As a next step, we would like to understand which of the used features are the strongest indicators of the presence of a ship in the area for the XGB model. For this, we perform the explainability analysis using the SHapley Additive exPlanations (SHAP) [19] summary plots (see Figure 6). The plots indicate the strength of the impact of a value of a certain model feature on the model outcome (positive or negative) for individual samples from the test set. The red and blue colors show the effects of the high and low values of a certain feature respectively.

We can see that for the Mediterranean Sea, and Biscay Bay, the feature having the strongest impact on the decision of the model the most is *scd std*, representing the standard deviation of stratospheric column density within the image patch. In the case of the Mediterranean Sea, *scd max* and *solar azimuth angle* also play significant roles. Interestingly, the direction of the meridional wind can also influence the model's decision in the Mediterranean Sea, with negative meridional wind corresponding to strongly negative model responses, potentially due to land outflow from Europe affecting ship plume visibility. In the Arabian Sea and Bengal Bay regions, the strongest impact on the model response is attributed to the values of the feature *scd mean*. Notably, for the Arabian Sea, high values of *scd std* do not necessarily indicate the presence of a plume, possibly because as we can see from Figure 7, standard deviations of NO_2 concentrations in this region are typically lower compared to others. Low values of *scd std*, however, are used by the model as a strong suggestion of the absence of a plume in the image patch. Finally, one can notice that for Biscay Bay, the feature *sensor zenith angle* is of great importance. However, since we do not see a clear split into high/low values for positive/negative model outcomes, the influence of the feature on the model response will depend on the values of other features [9, 12].

From this experiment, we can conclude that the same machine learning models applied to different studied regions not only yield different quality of results but are also driven by different sets of features.

3.2 RQ1: Tropomi sensitivity limits

3.2.1 Ship emission proxy – definition. In this Subsection, we address the first research question: What is the minimal speed/length of the seagoing ship so that the NO_2 plume from it can be detected with the TROPOMI/S5P instrument? In [10], it was shown that the length and the speed of the ship are the main factors determining the emission potential of the ship. Following the considerations presented in [10], in order to decrease the level of problem complexity, we represent the length/speed of the studied ship in terms of one variable – the ship emission proxy E_s [10] defined as:

$$E_s = L_s^2 \cdot u_s^3 \tag{1}$$

where L_s is the length of the ship in m and u_s is the speed of the ship in m/s. If there is more than one ship in the area covered by the image patch, the total emission proxy is computed as the sum of the E_s for all ships located in this area. For the purpose of this paper, we define the sensitivity limit of TROPOMI for a given region as the level of ship emission proxy E_s, starting from which the classification model is able to distinguish image patches without a ship from image patches with a ship.

3.2.2 The lowest emitters in the dataset. Therefore, as a first step, we check what is the performance of the classification model, when for the training/test we use the set of image patches with the lowest total emission proxy. For this experiment, we only selected the image patches with one ship on it. Then, among all one-ship patches, we only select those with an emission proxy below the 10% quantile of all one-ship patches. To make the performance metrics comparable, we sample from the image patches without any ship a number of data points equal to the number of selected patches left after applying the the 10% quantile threshold. To ensure a sufficient representation of no-ship patches, we repeat the sampling procedure 5 times. For each of the sampled sets of data points, we perform a 5-fold cross-validation. The results averaged over 5 folds of cross-validation performed for 5 sets of sampled sets of data are presented in Table 5. From the results, we can see that for none of

[4]All above-mentioned models are implemented in Python scikit-learn v.1.2.2.
[5]XGBoost v. 1.7.0
[6]Implemented in Python scikit-learn v.1.2.2.

Region	Model	Average Precision	ROC-AUC
Mediterranean	XGB	**0.614 ± 0.014**	**0.692 ± 0.011**
	Random Forest	0.603 ± 0.014	0.682 ± 0.013
	SVM (rbf)	0.601 ± 0.014	0.682 ± 0.011
	Logistic	0.445 ± 0.008	0.547 ± 0.009
Biscay Bay	XGB	**0.707 ± 0.014**	**0.717 ± 0.014**
	Random Forest	0.627 ± 0.023	0.661 ± 0.018
	SVM (rbf)	0.57 ± 0.019	0.588 ± 0.013
	Logistic	0.523 ± 0.012	0.541 ± 0.017
Arabian Sea	XGB	0.214 ± 0.006	0.6 ± 0.008
	Random Forest	**0.219 ± 0.005**	**0.606 ± 0.005**
	SVM (rbf)	0.185 ± 0.006	0.539 ± 0.009
	Logistic	0.163 ± 0.0	0.5 ± 0.0
Bengal Bay	XGB	**0.383 ± 0.012**	**0.617 ± 0.012**
	Random Forest	0.365 ± 0.016	0.601 ± 0.012
	SVM (rbf)	0.347 ± 0.003	0.562 ± 0.01
	Logistic	0.292 ± 0.009	0.545 ± 0.014

Table 4: Results of the optimization of the classification models' hyperparameter. The reported results were obtained on the hold-out test sets on the basis of nested 5-fold cross-validation [3, 23]. The bold font indicates the performance of the best model for a given region.

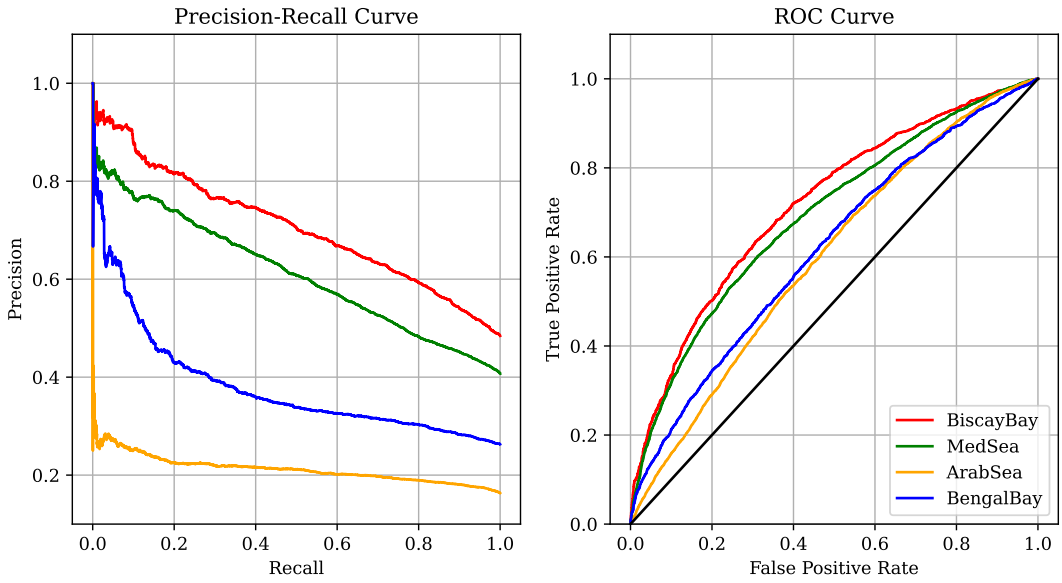

Figure 5: Precision-recall and ROC curves for the studied regions. Black line – performance of a random classifier.

Region	Average Precision	ROC-AUC
Mediterranean	0.542 ± 0.033	0.513 ± 0.038
Biscay Bay	0.551 ± 0.054	0.529 ± 0.061
Arabian Sea	0.564 ± 0.035	0.564 ± 0.321
Bengal Bay	0.553 ± 0.052	0.536 ± 0.053

Table 5: Model performance when only considering the one-ship patches with the emission proxy below 10% quantile.

the regions, the patches with a ship can be distinguished, as none of the obtained values of ROC-AUC are significantly higher than 0.5. We, therefore, conclude that the lowest E_s ships from our dataset are below the sensitivity limit of the TROPOMI satellite.

3.2.3 On TROPOMI sensitivity limits. In the next experiment, we check what the emission proxy threshold for the ship plumes detectability is. Here, we again consider only image patches with one

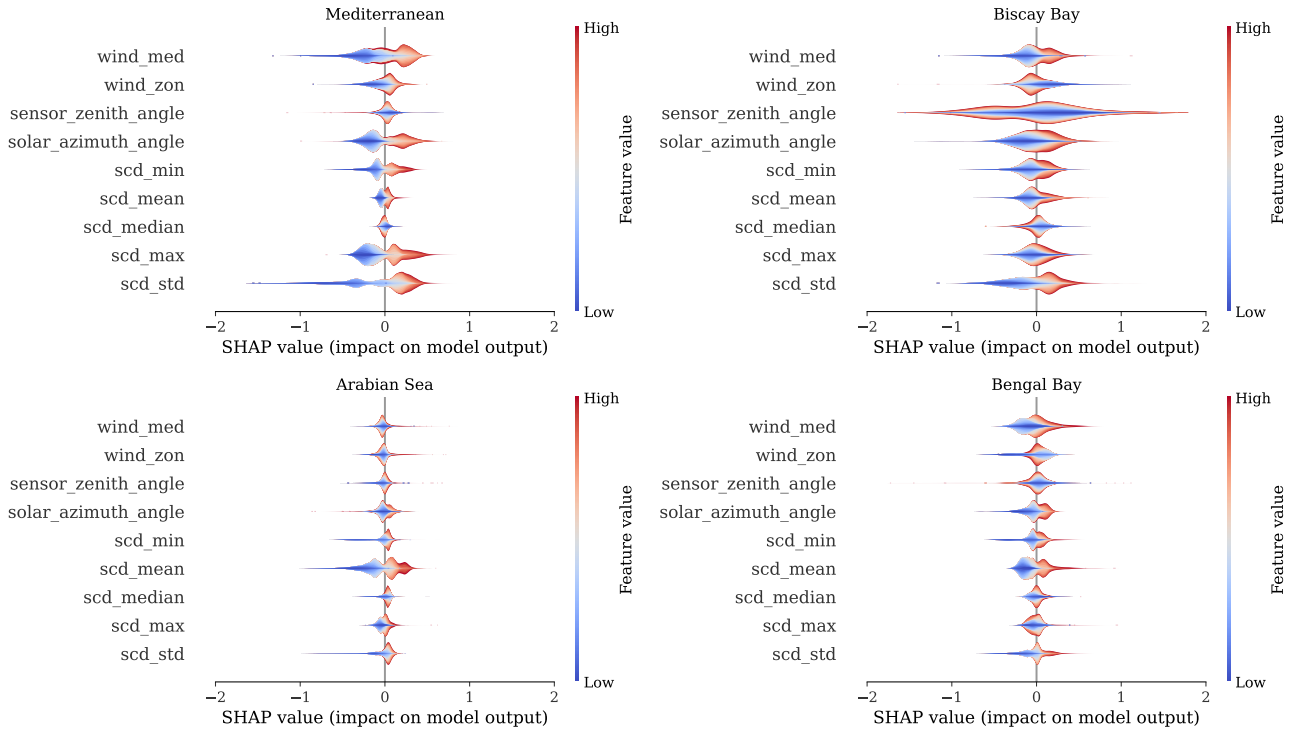

Figure 6: SHAP violin plots on concatenated test sets for each studied region.

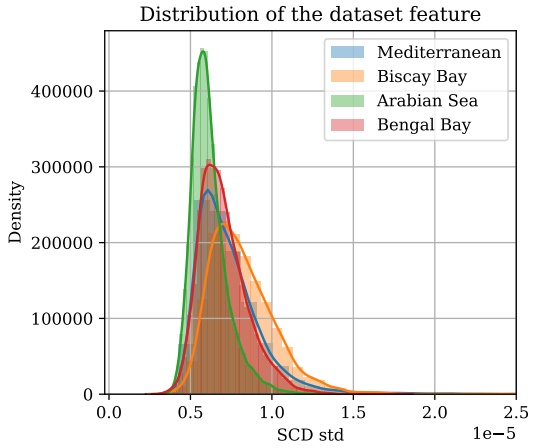

Figure 7: Distribution of the variable *scd std* for four studied regions. For the Arabian Sea, the distribution is noticeably more narrow than for other regions.

ship on it. We then gradually remove ships with the lowest emission proxy from the dataset, analyzing the changes in the model performance.

The applied emission proxy thresholds were determined as a range of quantiles starting from 10% and gradually increasing by 10%, until it reaches 90%. If after reaching a certain level of threshold, the number of patches with a ship (label 1) goes below 300, the experiment is terminated and the next thresholding levels are not tested[7]. The criterion of 300 patches was established based on the number of patches with a ship left after a 90% threshold applied for the region with the highest number of one-ship patches available (Arabian Sea).

Clearly, by removing the image patches with the proxy values below a certain threshold, we decrease the size of the dataset. To eliminate the potential effect of the dataset size on the model performance, throughout the experiment, we keep the dataset size constant. To achieve this, for each applied threshold, we sample the number of data points equal to the number of data points available for the highest applied threshold. As in the previous experiment, we repeat the sampling procedure 5 times. For each set of sampled data points, we perform a 5-fold cross-validation.

The results of the experiment are presented in Figure 8. We can see that for the lowest thresholds, for all four regions, the average performance quality does not change. This means that the removed ships were still below the sensitivity level of the satellite. From a certain threshold (indicated with a black line on the plot), however, for the regions of the Arabian and Mediterranean Seas, the model performance starts to grow. The level of ship emission proxy threshold starting from which we observe the improvement of the performance of the model is a sensitivity limit of a TROPOMI instrument for a given region. For the Mediterranean and Arabian Sea, the level of sensitivity limit is around $1 \times 10^7 m^5/s^3$. For those regions, in Figure 9, we present 2D histograms of the speed and

[7]This way, the highest applied threshold for Biscay Bay was 70% and for Bengal Bay 80% quantile.

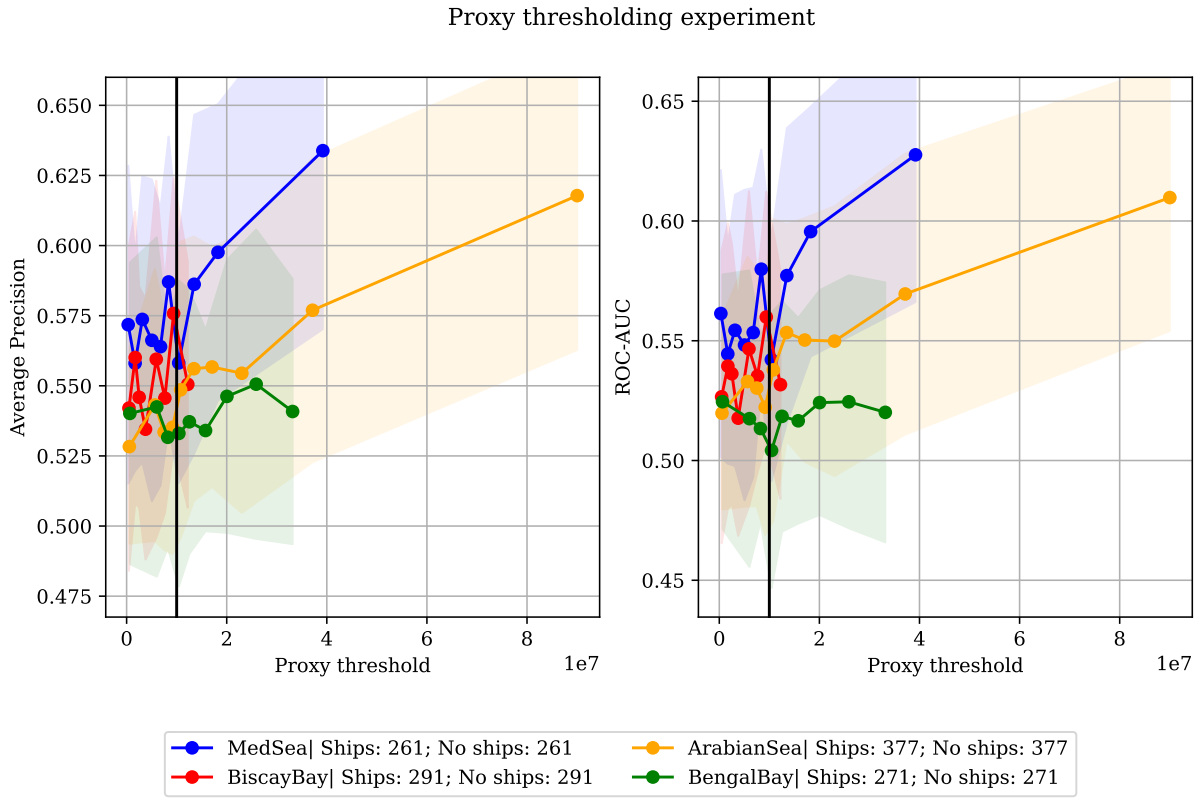

Figure 8: Step-wise removal of the patches (containing one ship) with the lowest emission proxy. Black lines indicate the estimated level of TROPOMI sensitivity limit for the Mediterranean and Arabian Seas. To assure the comparability of the results, a similar size of training/test datasets was used at each threshold level.

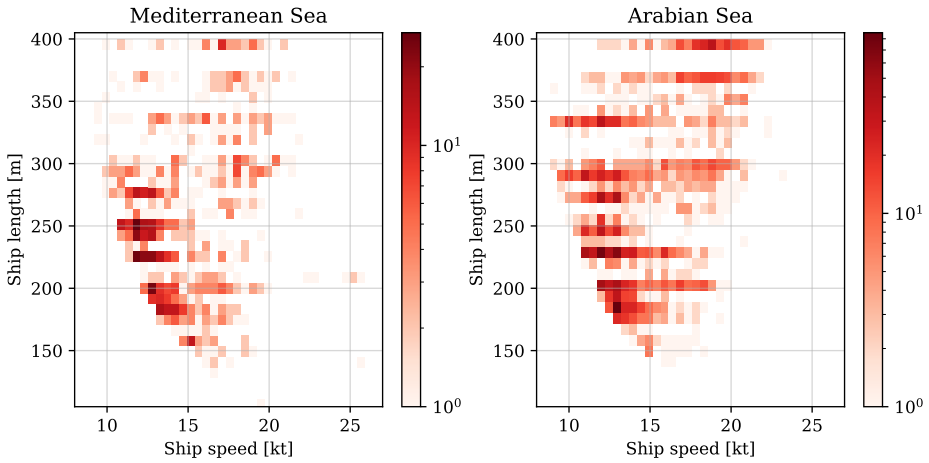

Figure 9: 2D histograms of speed and lengths for ships that are above the TROPOMI sensitivity limits for the Mediterranean Arabian Seas.

length of ships that are above the TROPOMI sensitivity limits. From the histograms, we conclude that in order NO_2 plumes to be possible to distinguish with TROPOMI, the minimal speed of the ship should range between 10 and 15 kt in dependence on the length of the ship. Ships that are slower than 10 kt or shorter than 150 are below the sensitivity limit of the TROPOMI satellite.

For the Biscay and Bengal Bays, the sensitivity limits cannot be determined due to the fact that the available amount of data did not allow us to raise the proxy threshold high enough to see the growth of the performance of the model. However, for Bengal Bay, when comparing to the curve dynamics of other regions, the obtained pattern suggests that the cut-off level is higher than for the Arabian and Mediterranean Seas.

3.3 RQ2: On detection of biggest emitters

Our second research question is how the detectability of NO_2 plumes can be improved if only the biggest emitters are taken into account. Our aim here is to understand what is the potential of the detectability of NO_2 plumes when the total emission proxy is very high. Therefore, in this experiment, we consider all image patches (without, with one, or with more than one ship on it). This way, in some of the image patches, there will be more than one ship with a high emission proxy present.

As in the previous experiment, we gradually remove from the dataset the image patches with the lowest total emission proxy. Once again we study how the removal of the low emitters affects the quality of classification. The thresholds used for the proxy filtering were determined as quantiles of the proxy values of the dataset of a given region. For the Mediterranean and Arabian Sea, the applied quantiles ranged from 0 to 90%. For the Biscay and Bengal Bay, due to the smaller sizes in the datasets, the applied quantiles ranged from 0 to 80%.

In Figure 10, we present the results of the experiment. For each of the studied regions, we can observe a growth in the model performances. We can see that for the Mediterranean and Biscay Bay for the patches with the highest total emission proxy, the ROC-AUC score can reach the high level of 0.8. For the regions Arabian Sea and Bengal Bay, the level of the results is noticeably lower. Such a pattern of the results is similar to what we observed in Subsection 3.1.

As a next step, we check if the dependency between the applied proxy threshold and classification performance is impacted by a certain hyperparameter configuration of the XGB model. We would like to know to which extent we can improve the quality of classification for the image patches with the highest total emission proxy. For this, we studied two configurations of the dataset. In the first case, we applied the highest proxy threshold for the given region (the last data point from the corresponding plots of Figure 10). In the second case, we did not apply any proxy threshold but kept the dataset size equal to the case when the proxy threshold was applied (the scenario corresponds to the first data point of the corresponding plots of Figure 10). For each of the datasets, we performed optimization of the hyperparameters of the classification model, in the same way as it is explained in 3.1. We then compared the performance of the models for both scenarios.

The results are presented in Figure 11. For all studied regions, we can see that the quality of detecting NO_2 plumes from ships can be improved if only the image patches with the highest total emission proxy are considered. We can see that for the regions of the Arabian Sea and Bengal Bay, the optimization of hyperparameters allowed us to gain some improvement in the model performance. For the Mediterranean Sea and Biscay Bay, the improvement of the model performance, if present, is not significant. Based on the presented above results, we can conclude that the dependencies shown in Figure 10 are not the results of a particular model configuration, but rather a property of data.

3.4 RQ3: On potential improvement of small ship detectability

In this Subsection, we address the third research question of the study. Namely, we investigate whether there is a potential for improvement of detectability of NO_2 plumes from the slow/small ships if more data would be used for the training of the classification model. For each region, we selected three proxy thresholding levels and studied the change in the model performance with the growth of the size of the dataset used for the model training. We focus here on the low thresholds. The used thresholds were set as 10%, 30%, and 50% quantiles of the proxy value for the Mediterranean Sea and Biscay Bay. For the Arab Sea and Bengal Bay, the applied thresholds were 10%, 40%, and 60% due to the fact that the model performances on the lowest quantiles were indistinguishable. Similarly to the previous experiment, the maximal size of the dataset was defined by the number of data points in the dataset with the proxy value higher than the highest among the three applied thresholds.

The resulting learning curves for each of the studied regions are presented in Figure 12. We can see that for all studied regions, the results shown in Figure 10 can be improved by using more data for model training. We also observe that for the regions Biscay Bay and Mediterranean Sea, more data results in a more significant increase in performance, than for the Arabian Sea and Bengal Bay. To explain this, in Figure 13, we present the distribution of the variable ship emission *Proxy* for each consecutive threshold applied. The histograms show that for the Biscay Bay and the Mediterranean Sea, there are many more image patches with high values of total emission proxy than for the Arabian Sea and Bengal Bay. As a result, even after removing from the dataset the image patches with the lowest total emission proxy, for such regions as the Arabian and Bengal Bay, the models are still trained on significantly lower total emission proxies than the models for the Biscay Bay and the Mediterranean Sea.

4 DISCUSSION

The main objective of this study was to investigate the sensitivity of the TROPOMI sensor in detecting NO_2 emissions from individual seagoing ships, considering their speed and length that we expressed through the means of ship emission proxy.

We addressed the problem of the sensitivity of the TROPOMI instrument with machine-learning classification models. This approach allowed us to effectively exploit the TROPOMI signal while automatically separating the image patches into those, where the

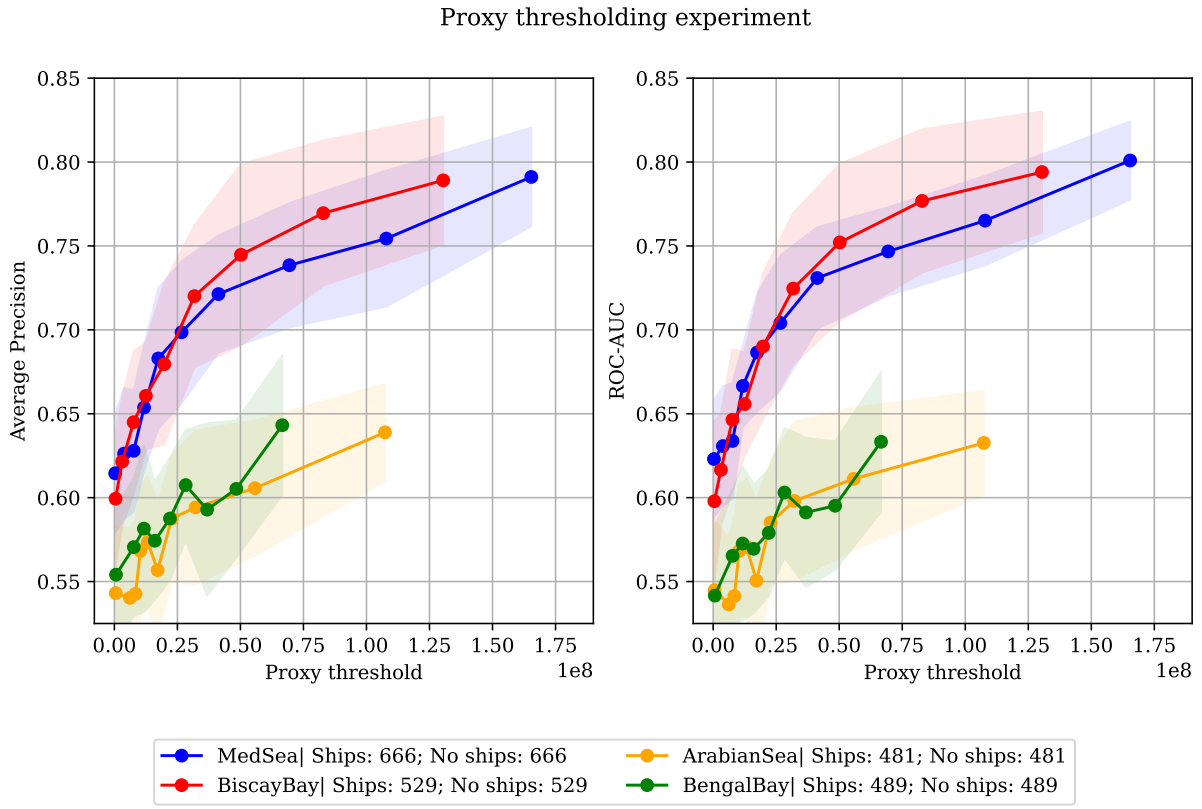

Figure 10: Illustration on how the step-wise removal of the image patches with the lowest total emission proxy from the dataset affects the performance of the classification model.

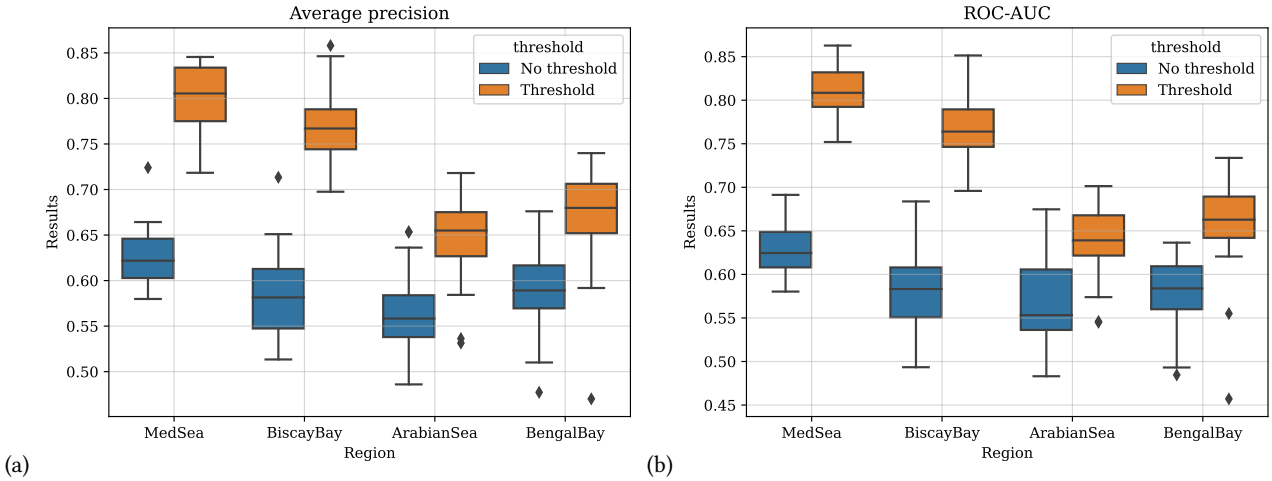

Figure 11: Comparison of the performance of the model when all ship images are in the dataset and when only images with the proxy above the predetermined proxy threshold are used.

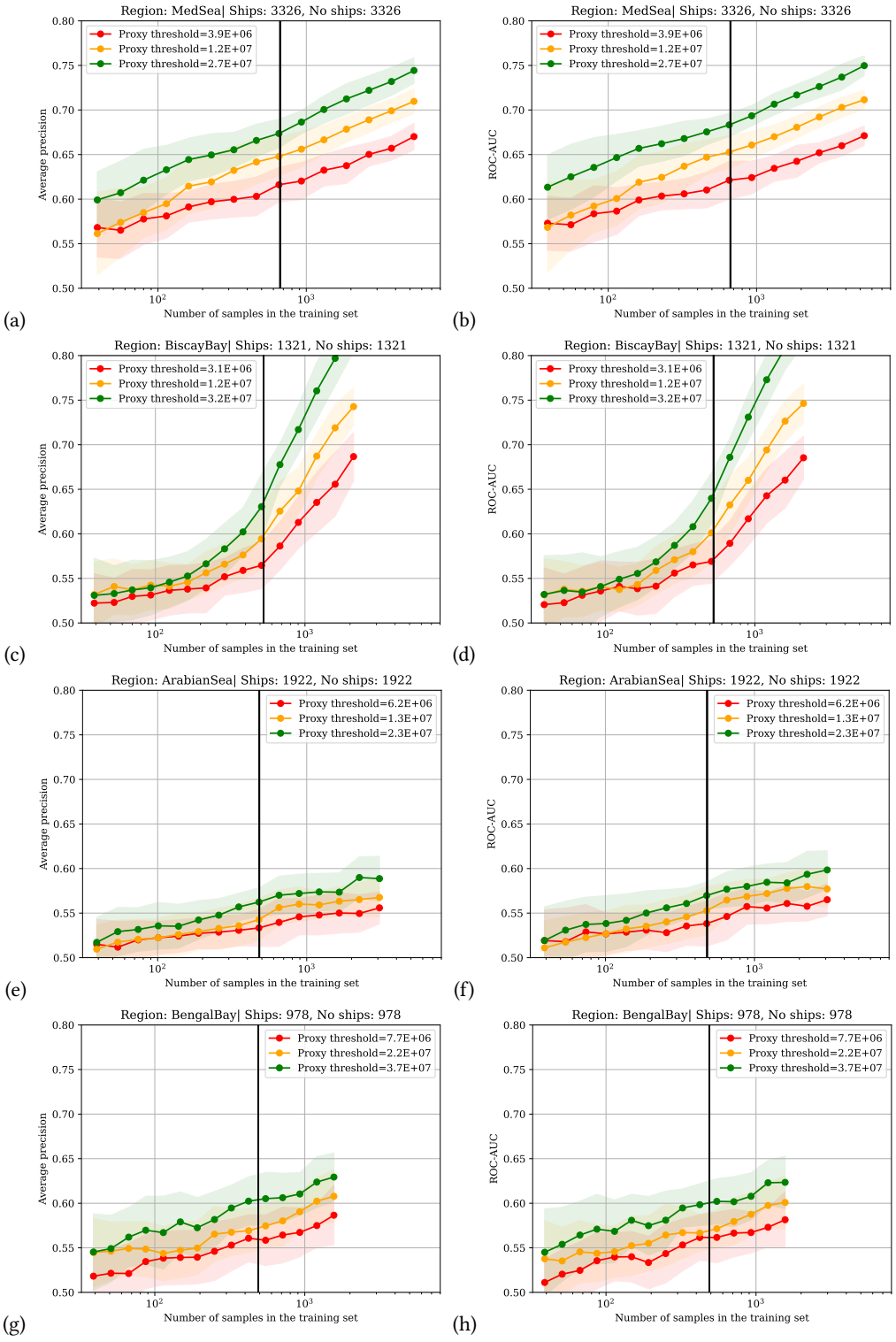

Figure 12: Learning curves for different levels of the applied thresholds. The black line indicates the dataset size that was used for the experiments reported in Figures 10, 11.

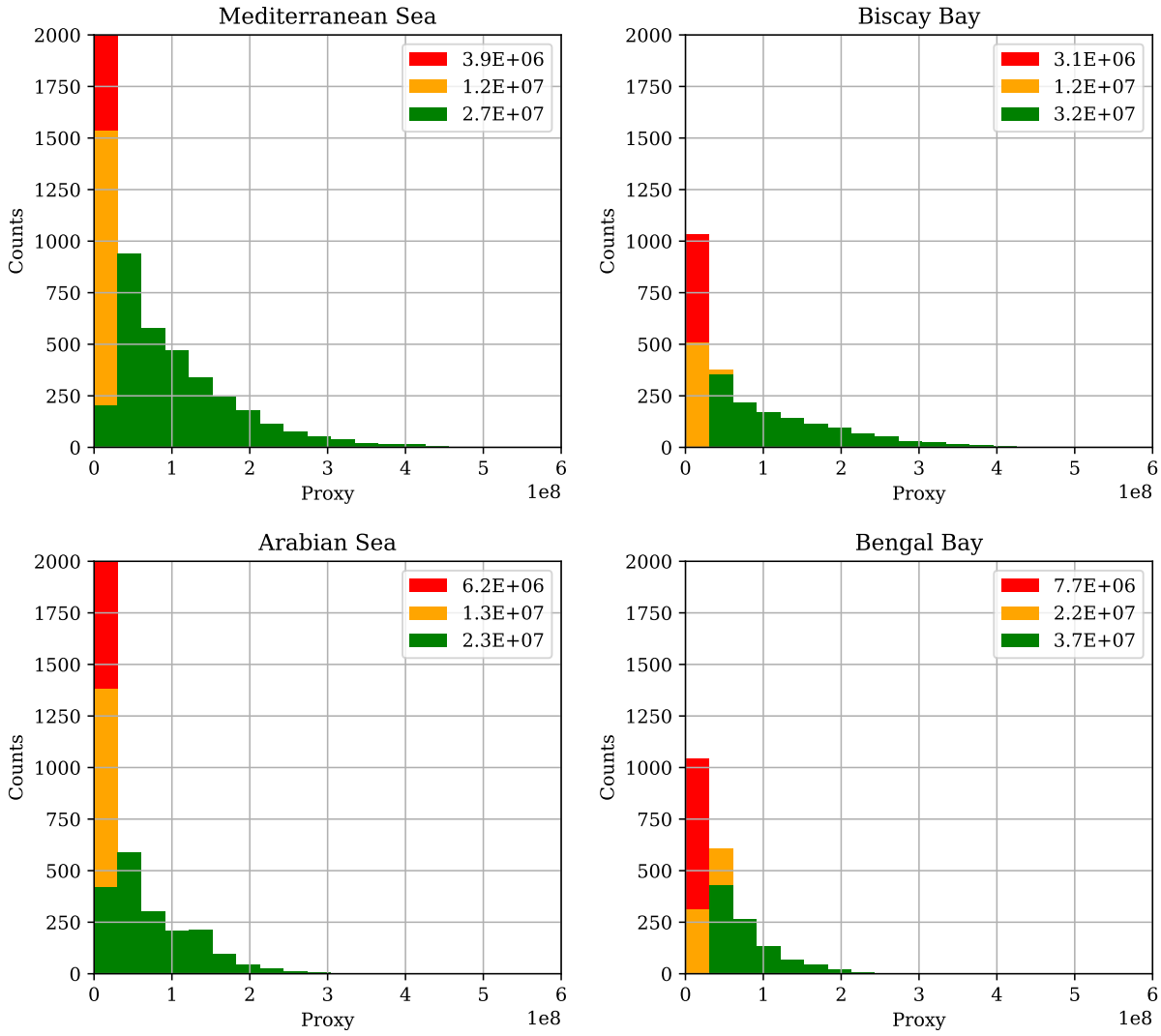

Figure 13: Change of the distribution of ship proxy as a result of applying thresholds as in Figure 12.

NO_2 plumes can and cannot be detected. The choice of a multivariate model enabled us to take into account features important for satellite sensitivity, such as wind and satellite/solar viewing angles. Studying several machine learning classifiers of increasing complexity, we found that the XGB model consistently yielded the best performance across most regions. This shows the importance of the application of complex machine-learning models for the effective identification of TROPOMI image patches with NO_2 plumes from ships with a relatively low number of features. The optimization of hyperparameters, though resulted in some improvement in model performance for two studied regions, did not have an influence on the obtained conclusions.

4.0.1 RQ1. With the first research question, we attempted to determine the minimal speed and length of seagoing ships for which the TROPOMI/S5P instrument can detect NO_2 plumes. We first showed that while the smallest ships considered in our dataset are below the detection limit of the instrument, once reaching a certain level of ship speed/size, the signal becomes detectable. Second, for the Mediterranean Sea and the Arabian Sea, we estimated sensitivity limits of approximately $1 \times 10^7 m^5/s^3$. Translating this into the speed and length of a ship, we conclude that ships that are slower than 10 kt or shorter than 150 are below the sensitivity limit of the TROPOMI satellite. Comparing those numbers with speed and length thresholds used in previous studies, we can see that previously applied thresholds were put higher than the actual detection limit of the satellite. Unfortunately, due to the insufficient amount of data, the sensitivity limits for the Biscay Bay and Bengal Bay regions could not be determined.

4.0.2 RQ2. With the second research question, we examined the potential improvement in NO_2 plume detectability when considering only the biggest emitters. Our results indicate that restricting the analysis to faster/larger ships leads to enhanced detectability of NO_2 plumes. For such regions as the Mediterranean Sea and Biscay Bay, the performance of the classification model can reach up to 0.8 ROC-AUC and average precision scores. This finding suggests concentrating the focus on the larger emitters, could potentially increase the efficiency of the application and accuracy of ship emission monitoring using the TROPOMI instrument. Our analysis also revealed distinct differences in model performance quality between regions. Notably, the Mediterranean Sea and Biscay Bay consistently show better performance compared to the Arabian Sea and Bengal Bay. We can see that these variations could partially be attributed to variations in ship traffic density between the regions. However, it could also be an effect of local atmospheric characteristics, or other factors affecting satellite sensitivity.

4.0.3 RQ3. Our investigation into the third research question, regarding the potential for improving NO_2 plume detectability from slow or small ships by utilizing more training data, again showed the variability of the results across the regions. For the Mediterranean Sea and Biscay Bay regions, an increase in data volume led to a notable enhancement in model performance. While, for the Arabian Sea and Bengal Bay, the impact of increased data, even though present, was less pronounced. One of the established reasons was the fact that for European regions we had a higher ratio of data points with a high value of emission proxy in the dataset than for the Bengal Bay and Arabian Sea. Nevertheless, the obtained results provide an indication that the accuracy of currently determined detection limits is perhaps constrained not by the methodology or the sensor, but by data availability.

4.0.4 Implications and future work. The insights gained from this study have important implications for satellite-based ship emission monitoring. By identifying sensitivity limits and optimal ship characteristics for detectability, our findings provide guidance regarding the scope of future studies on ship's NO_2 estimation using TROPOMI data and give an overview of the potential application of the TROPOMI instrument for ship emission monitoring. Moreover, the obtained results can be used as a benchmark sensitivity level for future satellite missions, such as, for instance, TANGO [18].

In future research, it would be valuable to explore factors beyond ship speed and length that influence detectability, such as atmospheric conditions, or satellite viewing angles. Moreover, it would be valuable to perform an in-depth study explaining the observed multi-regional differences in ship plume detectability. Finally, studying different types of machine-learning architectures can provide insights into understanding if the ship plume detectability limits can be lowered further by means of potential improvement information extraction from image patches. A possible candidate is Convolutional Neural Networks (CNN), as it was done in [8] for detection of visually distinguishable ship NO_2 plumes. However, [16, 17] provide indications that CNN architecture might not be a suitable option for ship plume detection at the edge of the TROPOMI sensitivity limit.

5 CONCLUSIONS

In this study, we investigated the sensitivity limits of the TROPOMI satellite with respect to the detection of NO_2 plumes from individual seagoing ships. To the best of our knowledge, no previous research has examined this aspect, making our findings novel and significant in understanding the capabilities of the TROPOMI/S5P instrument. Our results are obtained through the analysis of four regions of interest (the Mediterranean Sea, Biscay Bay, Arabian Sea, and Bengal Bay) and can be summarized as follows:

(1) We quantified the TROPOMI sensitivity limit in terms of length and speed of a ship beyond which the NO_2 plumes from individual ships cannot be distinguished anymore.
(2) We also showed that, as expected, the ships with higher emissions (through either greater length or speed) are more easily detected. We demonstrated such an effect by analyzing model performances with the removal from the dataset ships with the lowest emission proxy. This is agnostic to the model or studied region.
(3) We also demonstrated that the detection of the NO_2 plumes from the ships with lower emission proxy can be improved, once more training data is added.
(4) Finally, we obtained different levels of results between the studied regions. We showed that for different regions a machine learning model not only yields different levels of results but also uses different features as indicators of the presence of a plume in an image patch. A discrepancy is noticeable when comparing the Arabian Sea and Bengal Bay to the Mediterranean Sea and Biscay Bay.

To sum up, our findings suggest that, while efficient monitoring of seagoing ships from the TROPOMI satellite is possible, the quality of ship plume detectability depends on many factors. We believe our results provide guidelines for establishing the research scope for future studies on NO_2 ship plume detection as well as contribute to the successful application of satellite-based instruments for the monitoring of NO_2 emission from seagoing ships.

ACKNOWLEDGMENTS

We would like to express our sincere gratitude to Charles Moussa for fruitful discussions and help with the implementation of some of the experiments presented in this study. This work is funded by the Netherlands Human Environment and Transport Inspectorate, the Dutch Ministry of Infrastructure and Water Management, and the SCIPPER project, which receives funding from the European Union's Horizon 2020 research and innovation program under grant agreement Nr.814893.

REFERENCES

[1] Harshit Agrawal, Quentin GJ Malloy, William A Welch, J Wayne Miller, and David R Cocker III. 2008. In-use gaseous and particulate matter emissions from a modern ocean going container vessel. *Atmospheric Environment* 42, 21 (2008), 5504–5510. https://doi.org/10.1016/j.atmosenv.2008.02.053

[2] Jörg Beecken, Johan Mellqvist, Kent Salo, Johan Ekholm, and J-P Jalkanen. 2014. Airborne emission measurements of SO 2, NO x and particles from individual ships using a sniffer technique. *Atmospheric Measurement Techniques* 7, 7 (2014), 1957–1968. https://doi.org/10.5194/amt-7-1957-2014

[3] Gavin C Cawley and Nicola LC Talbot. 2010. On over-fitting in model selection and subsequent selection bias in performance evaluation. *The Journal of Machine Learning Research* 11 (2010), 2079–2107. https://doi.org/10.5555/1756006.1859921

[4] Tianqi Chen and Carlos Guestrin. 2016. Xgboost: A scalable tree boosting system. In *Proceedings of the 22nd acm sigkdd international conference on knowledge discovery and data mining*. 785–794. https://doi.org/10.1145/2939672.2939785

[5] James J Corbett, James J Winebrake, Erin H Green, Prasad Kasibhatla, Veronika Eyring, and Axel Lauer. 2007. Mortality from ship emissions: a global assessment. *Environmental science & technology* 41, 24 (2007), 8512–8518. https://doi.org/10.1021/es071686z

[6] Henk Eskes, Jos van Geffen, Folkert Boersma, Kai-Uwe Eichmann, Arnoud Apituley, Mattia Pedergnana, Maarten Sneep, J. Pepijn Veefkind, and Diego Loyola. 2022. *Sentinel-5 precursor/TROPOMI Level 2 Product User Manual Nitrogendioxide.* Technical Report S5P-KNMI-L2-0021-MA.

[7] Pedregosa Fabian. 2011. Scikit-learn: Machine learning in Python. *Journal of machine learning research 12* (2011), 2825. https://doi.org/10.5555/1953048.2078195

[8] Douglas P Finch, Paul I Palmer, and Tianran Zhang. 2022. Automated detection of atmospheric NO 2 plumes from satellite data: a tool to help infer anthropogenic combustion emissions. *Atmospheric Measurement Techniques* 15, 3 (2022), 721–733. https://doi.org/10.5194/amt-15-721-2022

[9] Jerome H Friedman and Bogdan E Popescu. 2008. Predictive learning via rule ensembles. (2008). https://doi.org/10.1214/07-AOAS148

[10] Aristeidis K Georgoulias, K Folkert Boersma, Jasper van Vliet, Xiumei Zhang, Prodromos Zanis, Jos de Laat, et al. 2020. Detection of NO2 pollution plumes from individual ships with the TROPOMI/S5P satellite sensor. *Environmental Research Letters* 15, 12 (2020), 124037. https://doi.org/10.1088/1748-9326/abc445

[11] Aurélien Géron. 2022. *Hands-on machine learning with Scikit-Learn, Keras, and TensorFlow.* " O'Reilly Media, Inc.".

[12] Trevor Hastie, Robert Tibshirani, Jerome H Friedman, and Jerome H Friedman. 2009. *The elements of statistical learning: data mining, inference, and prediction.* Vol. 2. Springer. https://doi.org/10.1007/978-0-387-21606-5

[13] IMO. 1997. Amendments to the annex of the protocol of 1978 relating to the international convention for the prevention of pollution from ships. https://wwwcdn.imo.org/localresources/en/KnowledgeCentre/IndexofIMOResolutions/MEPCDocuments/MEPC.75(40).pdf

[14] IMO. 2020. MARPOL ANNEX VI - regulation 13. https://www.imo.org/en/OurWork/Environment/Pages/Nitrogen-oxides-(NOx)-%E2%80%93-Regulation-13.aspx

[15] Solomiia Kurchaba, Jasper van Vliet, Jacqueline J Meulman, Fons J Verbeek, and Cor J Veenman. 2021. Improving evaluation of NO2 emission from ships using spatial association on TROPOMI satellite data. In *29th International Conference on Advances in Geographic Information Systems*. 454–457. https://doi.org/10.1145/3474717.3484213

[16] Solomiia Kurchaba, Jasper van Vliet, Fons J. Verbeek, Jacqueline J. Meulman, and Cor J. Veenman. 2022. Supervised Segmentation of NO2 Plumes from Individual Ships Using TROPOMI Satellite Data. *Remote Sensing* 14, 22 (2022). https://doi.org/10.3390/rs14225809

[17] Solomiia Kurchaba, Jasper van Vliet, Fons J Verbeek, and Cor J Veenman. 2023. Anomalous NO2 emitting ship detection with TROPOMI satellite data and machine learning. *Remote Sensing of Environment* 297 (2023), 113761.

[18] Jochen Landgraf, Stephanie Rusli, Ryan Cooney, Pepijn Veefkind, Tim Vemmix, Zeger de Groot, Andrew Bell, James Day, Anton Leemhuis, and Bernd Sierk. 2020. The TANGO mission: A satellite tandem to measure major sources of anthropogenic greenhouse gas emissions. In *EGU General Assembly Conference Abstracts*. 19643.

[19] Scott M Lundberg and Su-In Lee. 2017. A unified approach to interpreting model predictions. *Advances in neural information processing systems* 30 (2017).

[20] Robert McLaren, Patryk Wojtal, Jamie D Halla, Cris Mihele, and Jeffrey R Brook. 2012. A survey of NO2: SO2 emission ratios measured in marine vessel plumes in the Strait of Georgia. *Atmospheric environment* 46 (2012), 655–658. https://doi.org/10.1016/j.atmosenv.2011.10.044

[21] Jun Min Mou, Cees Van der Tak, and Han Ligteringen. 2010. Study on collision avoidance in busy waterways by using AIS data. *Ocean Engineering* 37, 5-6 (2010), 483–490. https://doi.org/10.1016/j.oceaneng.2010.01.012

[22] Maarten Sneep. 2021. *Sentinel 5 precursor/TROPOMI KNMI and SRON level 2 Input Output Data Definition.* Technical Report S5P-KNMI-L2-0009-SD.

[23] Mervyn Stone. 1974. Cross-validation and multinomial prediction. *Biometrika* 61, 3 (1974), 509–515. https://doi.org/10.1093/biomet/61.3.509

[24] W Van Roy and K Scheldeman. 2016. Results MARPOL Annex VI Monitoring Report: Belgian Sniffer Campaign 2016. (2016).

[25] JP Veefkind, I Aben, K McMullan, H Förster, J De Vries, G Otter, J Claas, HJ Eskes, JF De Haan, Q Kleipool, et al. 2012. TROPOMI on the ESA Sentinel-5 Precursor: A GMES mission for global observations of the atmospheric composition for climate, air quality and ozone layer applications. *Remote sensing of environment* 120 (2012), 70–83. https://doi.org/10.1016/j.rse.2011.09.027

[26] Geert CM Vinken, K Folkert Boersma, Daniel J Jacob, and Ernst W Meijer. 2011. Accounting for non-linear chemistry of ship plumes in the GEOS-Chem global chemistry transport model. *Atmospheric Chemistry and Physics* 11, 22 (2011), 11707–11722. https://doi.org/10.5194/acp-11-11707-2011

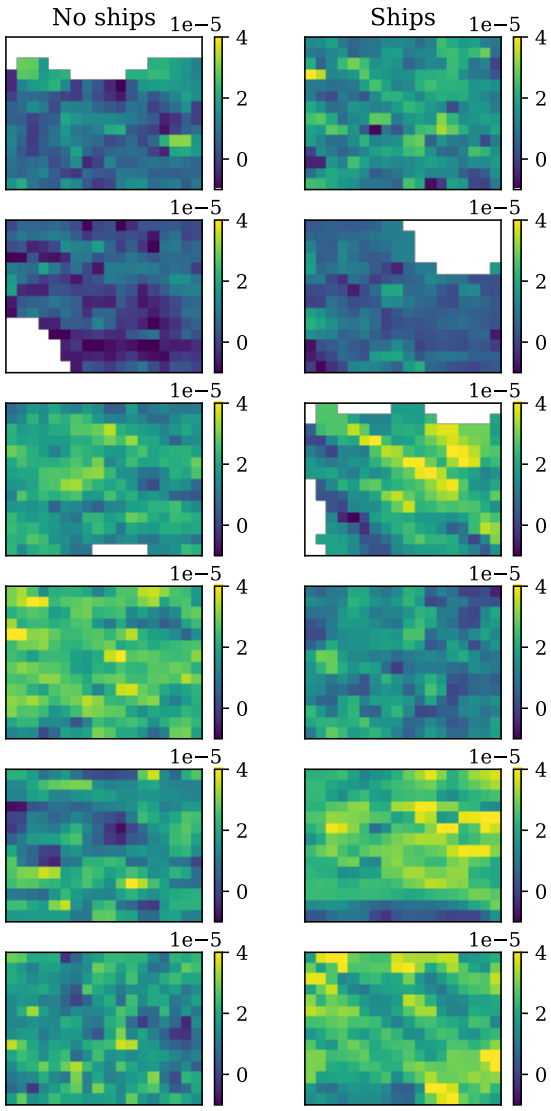

Figure 14: Examples of image patches without a ship and with at least one ship on it. The presented image patches were randomly sampled from the dataset of the region Biscay Bay.

Appendices

Appendix A EXAMPLES OF IMAGE PATCHES

In Figure 14, we present examples of image patches with and without ships that were used for the preparation of the dataset for this study.

Appendix B DATA DISTRIBUTIONS

In Figure 15, we provide the distribution of the features that are used in the dataset of this study.

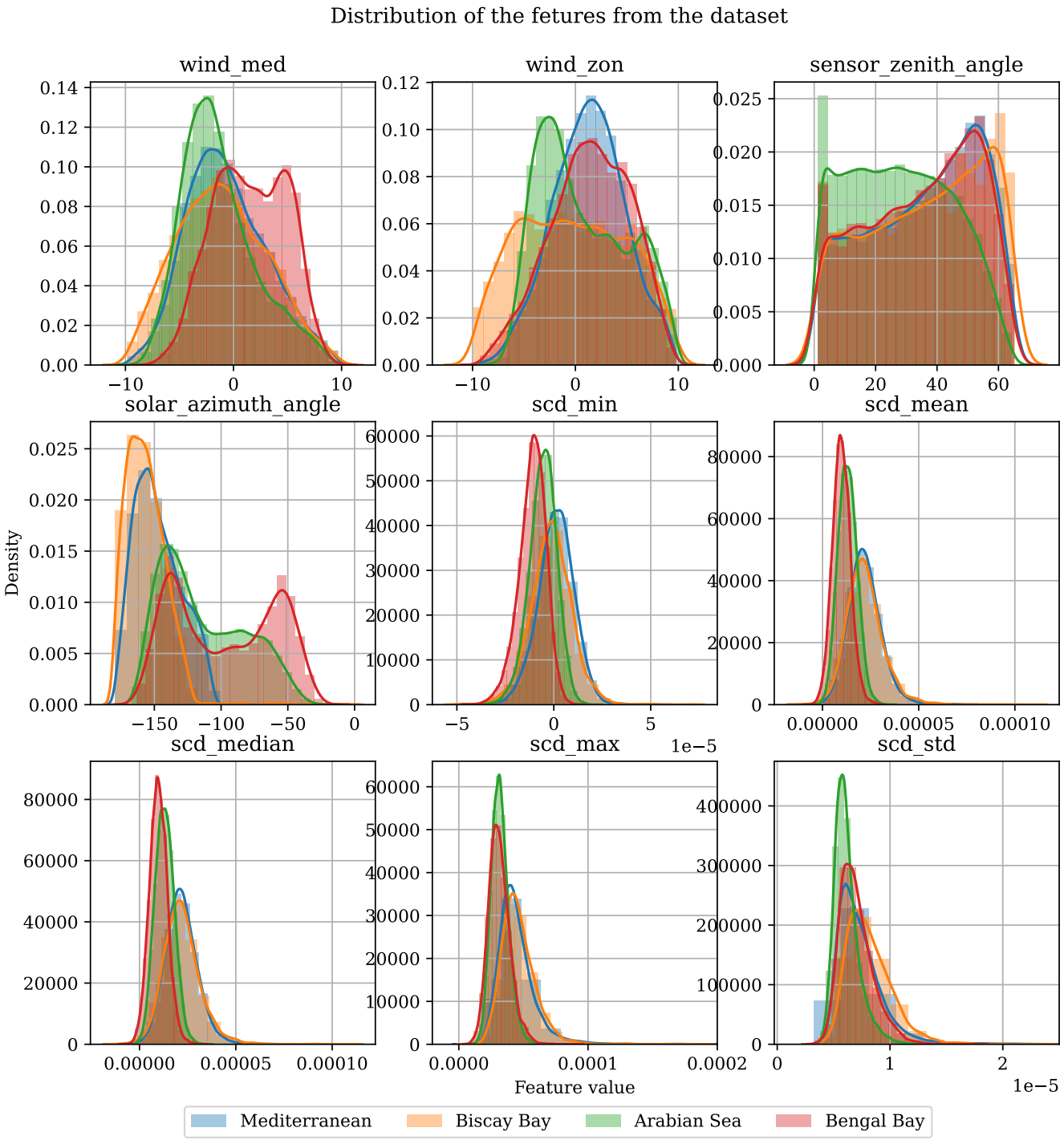

Figure 15: Histograms of the variables from the dataset.

Appendix C HYPERPARAMETERS' SEARCH SPACE

In this Section of the Appendix, we provide the hyperparameters' search space used for the optimization of the performance of the model.

- **Logistic**(solver='saga', l1_ratio=0.5, random_state=0)
  - penalty: ('l1', 'l2', 'elasticnet', 'none')
  - C: (0.0001, 0.001, 0.1, 1)
  - max_iter: (100, 120, 150)
- **SVM**(kernel='rbf', gamma = 'scale', random_state=0, probability=True)
  - C: (2.0e-2, 0.5e-1, 1.0e-1, 1.5e-1, 2.0e-1, 2.5e-1, 2.0)
- **Random Forest**(random_state=0)
  - n_estimators: [10, 20, 50, 100, 150, 500]
  - min_samples_leaf: [2; 36]
  - min_samples_split: [2, 30]
  - max_features: ('sqrt', 0.4, 0.5)
  - criterion: ('gini', 'entropy')
  - bootstrap: (True, False)
- **XGB**(random_state=0)
  - n_estimators: [10, 20, 50, 100, 150, 500]
  - gamma: [0.05; 0.5]
  - max_depth: (2, 3, 5, 6)
  - min_child_weight: (2, 4, 6, 8, 10, 12)
  - subsample: [0.6; 1.0]
  - learning_rate: [1e-3, 1e-2, 1e-1, 0.5, 1.0]
  - reg_alpha: (0, 1.0e-5, 5.0e-4, 1.0e-3, 1.0e-2, 0.1, 1)

Appendix D OPTIMIZED SET OF HYPERPARAMETERS

Then, we provide the set of hyperparameters that was selected as optimal for each model at each iteration of cross-validation for each studied region. The results of the performance of the corresponding models are presented in Table 4.

Mediterranean Sea

- **Logistic**(solver='saga', l1_ratio=0.5, random_state=0)
  - **penalty:** CV1: 'l1'; CV2: 'l2'; CV3: 'l2'; CV4: 'l2'; CV5: 'l2';
  - **C:** CV1: 0.1; CV2: 0.1; CV3: 0.001; CV4: 0.1; CV5: 1;
  - **max_iter:** CV1: 100; CV2: 100; CV3: 100; CV4: 100; CV5: 150;
- **SVM**(kernel='rbf', gamma = 'scale', random_state=0, probability=True)
  - **C:** CV1: 2; CV2: 2; CV3: 2; CV4: 2; CV5: 2;
- **Random Forest**(random_state=0)
  - **n_estimators:** CV1: 500; CV2: 500; CV3: 500; CV4: 500; CV5: 500;
  - **min_samples_split:** CV1: 7; CV2: 7; CV3: 7; CV4: 7; CV5: 12;
  - **min_samples_leaf:** CV1: 7; CV2: 7; CV3: 7; CV4: 7; CV5: 1;
  - **max_features:** CV1: 'sqrt'; CV2: 'sqrt'; CV3: 'sqrt'; CV4: 'sqrt'; CV5: 'sqrt';
  - **criterion:** CV1: 'entropy'; CV2: 'entropy'; CV3: 'entropy'; CV4: 'entropy'; CV5: 'gini';
  - **bootstrap:** CV1: True; CV2: True; CV3: True; CV4: True; CV5: True;
- **XGB**(random_state=0)
  - **n_estimators:** CV1: 500; CV2: 500; CV3: 500; CV4: 500; CV5: 500;
  - **gamma:** CV1: 0.3; CV2: 0.3; CV3: 0.05; CV4: 0.3; CV5: 0.05;
  - **max_depth:** CV1: 6; CV2: 6; CV3: 6; CV4: 6; CV5: 6;
  - **min_child_weight:** CV1: 8; CV2: 8; CV3: 10; CV4: 8; CV5: 10;
  - **subsample:** CV1: 0.6; CV2: 0.6; CV3: 0.7; CV4: 0.6; CV5: 0.7;
  - **learning_rate:** CV1: 0.01; CV2: 0.01; CV3: 0.01; CV4: 0.01; CV5: 0.01;
  - **reg_alpha:** CV1: 1e-05; CV2: 1e-05; CV3: 5e-04; CV4: 1e-05; CV5: 5e-04;

Biscay Bay

- **Logistic**(solver='saga', l1_ratio=0.5, random_state=0)
  - **penalty:** CV1: 'none'; CV2: 'l2'; CV3: 'l2'; CV4: 'elasticnet'; CV5: 'none';
  - **C:** CV1: 1e-4; CV2: 0.1; CV3: 1; CV4: 1; CV5: 1e-4;
  - **max_iter:** CV1: 100; CV2: 100; CV3: 100; CV4: 100; CV5: 150;
- **SVM**(kernel='rbf', gamma = 'scale', random_state=0, probability=True)
  - **C:** CV1: 2; CV2: 2; CV3: 2; CV4: 2; CV5: 2;
- **Random Forest**(random_state=0)
  - **n_estimators:** CV1: 500; CV2: 100; CV3: 500; CV4: 500; CV5: 150;
  - **min_samples_split:** CV1: 22; CV2: 2; CV3: 22; CV4: 22; CV5: 27;
  - **min_samples_leaf:** CV1: 10; CV2: 7; CV3: 10; CV4: 10; CV5: 10;
  - **max_features:** CV1: None; CV2: None; CV3: None; CV4: None; CV5: None;
  - **criterion:** CV1: 'entropy'; CV2: 'entropy'; CV3: 'entropy'; CV4: 'entropy'; CV5: 'entropy';
  - **bootstrap:** CV1: True; CV2: True; CV3: True; CV4: True; CV5: True;
- **XGB**(random_state=0)
  - **n_estimators:** CV1: 150; CV2: 150; CV3: 100; CV4: 100; CV5: 100;
  - **gamma:** CV1: 0.05; CV2: 0.05; CV3: 0.4; CV4: 0.4; CV5: 0.4;
  - **max_depth:** CV1: 6; CV2: 6; CV3: 6; CV4: 6; CV5: 6;
  - **min_child_weight:** CV1: 8; CV2: 8; CV3: 2; CV4: 2; CV5: 2;
  - **subsample:** CV1: 0.89; CV2: 0.89; CV3: 0.89; CV4: 0.89; CV5: 0.89;
  - **learning_rate:** CV1: 0.1; CV2: 0.1; CV3: 0.1; CV4: 0.1; CV5: 0.1;
  - **reg_alpha:** CV1: 1e-02; CV2: 1e-02; CV3: 1e-01; CV4: 1e-01; CV5: 1e-01;

Arabian Sea

- **Logistic**(solver='saga', l1_ratio=0.5, random_state=0)

  - **penalty:** CV1: 'l1'; CV2: 'l1'; CV3: 'l1'; CV4: 'l1'; CV5: 'l1';
  - **C:** CV1: 0.0001; CV2: 0.0001; CV3: 0.0001; CV4: 0.0001; CV5: 0.0001;
  - **max_iter:** CV1: 150; CV2: 120; CV3: 120; CV4: 120; CV5: 120;
- **SVM**(kernel='rbf', gamma = 'scale', random_state=0, probability=True)
  - **C:** CV1: 2; CV2: 0.25; CV3: 0.1; CV4: 2; CV5: 2;
- **Random Forest**(random_state=0)
  - **n_estimators:** CV1: 500; CV2: 500; CV3: 150; CV4: 500; CV5: 500;
  - **min_samples_split:** CV1: 22; CV2: 22; CV3: 12; CV4: 2; CV5: 2;
  - **min_samples_leaf:** CV1: 10; CV2: 10; CV3: 19; CV4: 16; CV5: 16;
  - **max_features:** CV1: None; CV2: None; CV3: None; CV4: 'sqrt'; CV5: 'sqrt';
  - **criterion:** CV1: 'entropy'; CV2: 'entropy'; CV3: 'entropy'; CV4: 'entropy'; CV5: 'entropy';
  - **bootstrap:** CV1: True; CV2: True; CV3: True; CV4: True; CV5: True;
- **XGB**(random_state=0)
  - **n_estimators:** CV1: 500; CV2: 500; CV3: 500; CV4: 500; CV5: 500;
  - **gamma:** CV1: 0.4; CV2: 0.2; CV3: 0.3; CV4: 0.05; CV5: 0.05;
  - **max_depth:** CV1: 6; CV2: 6; CV3: 6; CV4: 6; CV5: 6;
  - **min_child_weight:** CV1: 6; CV2: 2; CV3: 10; CV4: 10; CV5: 10;
  - **subsample:** CV1: 0.89; CV2: 0.89; CV3: 0.6; CV4: 0.7; CV5: 0.7;
  - **learning_rate:** CV1: 0.01; CV2: 0.01; CV3: 0.01; CV4: 0.01; CV5: 0.01;
  - **reg_alpha:** CV1: 5e-04; CV2: 1e-01; CV3: 1e-05; CV4: 5e-04; CV5: 5e-04;

Bengal Bay

- **Logistic**(solver='saga', l1_ratio=0.5, random_state=0)
  - **penalty:** CV1: 'l2'; CV2: 'elasticnet'; CV3: 'l2'; CV4: 'l1'; CV5: 'l1';
  - **C:** CV1: 1; CV2: 1; CV3: 0.001; CV4: 1; CV5: 1;
  - **max_iter:** CV1: 150; CV2: 150; CV3: 100; CV4: 150; CV5: 150;
- **SVM**(kernel='rbf', gamma = 'scale', random_state=0, probability=True)
  - **C:** CV1: 2; CV2: 0.25; CV3: 0.2; CV4: 0.05; CV5: 0.2;
- **Random Forest**(random_state=0)
  - **n_estimators:** CV1: 500; CV2: 500; CV3: 150; CV4: 150; CV5: 500;
  - **min_samples_split:** CV1: 2; CV2: 2; CV3: 12; CV4: 12; CV5: 2;
  - **min_samples_leaf:** CV1: 16; CV2: 16; CV3: 19; CV4: 19; CV5: 16;
  - **max_features:** CV1: 'sqrt'; CV2: 'sqrt'; CV3: None; CV4: None; CV5: 'sqrt';
  - **criterion:** CV1: 'entropy'; CV2: 'entropy'; CV3: 'entropy'; CV4: 'entropy'; CV5: 'entropy';
  - **bootstrap:** CV1: True; CV2: True; CV3: True; CV4: True; CV5: True;
- **XGB**(random_state=0)
  - **n_estimators:** CV1: 500; CV2: 150; CV3: 500; CV4: 500; CV5: 500;
  - **gamma:** CV1: 0.05; CV2: 0.15; CV3: 0.3; CV4: 0.3; CV5: 0.3;
  - **max_depth:** CV1: 6; CV2: 3; CV3: 6; CV4: 6; CV5: 6;
  - **min_child_weight:** CV1: 10; CV2: 6; CV3: 8; CV4: 8; CV5: 8;
  - **subsample:** CV1: 0.7; CV2: 0.79; CV3: 0.6; CV4: 0.6; CV5: 0.6;
  - **learning_rate:** CV1: 0.01; CV2: 0.1; CV3: 0.01; CV4: 0.01; CV5: 0.01;
  - **reg_alpha:** CV1: 5e-04; CV2: 1; CV3: 1e-05; CV4: 1e-05; CV5: 1e-05;